

# Channel Modeling and Channel Estimation for Holographic Massive MIMO with Planar Arrays

Özlem Tuğçe Demir, *Member, IEEE*, Emil Björnson, *Senior Member, IEEE*, Luca Sanguinetti, *Senior Member, IEEE*

**Abstract**—In a realistic wireless environment, the multi-antenna channel usually exhibits spatially correlation fading. This is more emphasized when a large number of antennas is densely deployed, known as holographic massive MIMO (multiple-input multiple-output). In the first part of this letter, we develop a channel model for holographic massive MIMO by considering both non-isotropic scattering and directive antennas. With a large number of antennas, it is difficult to obtain full knowledge of the spatial correlation matrix. In this case, channel estimation is conventionally done using the least-squares (LS) estimator that requires no prior information of the channel statistics or array geometry. In the second part of this letter, we propose novel channel estimation schemes that exploit the array geometry to identify a subspace of reduced rank that covers the eigenspace of any spatial correlation matrix. The proposed estimators outperform the LS estimator, without using channel statistics, and provide different performance/complexity tradeoffs.

**Index Terms**—Holographic massive MIMO, channel estimation, spatial correlation matrix, planar arrays.

## I. INTRODUCTION

The base stations (BSs) in 5G are equipped with a large number of antennas to enable efficient beamforming and spatial multiplexing of user equipments (UEs) [1]. This is known as massive MIMO (multiple-input multiple-output) [2] and the spectral efficiency increases with the number of antennas. The asymptotic performance limits have received much attention in the literature, under the assumption that the array aperture grows large. However, in practice, the array aperture is limited. Hence, the corresponding asymptotic limit is a spatially-continuous aperture with densely deployed antennas, known as *holographic MIMO* [3], [4] and large intelligent surface [5]. We will use the term *holographic massive MIMO* since it is a natural extension of current massive MIMO technology.

One way to approximately realize a spatially-continuous aperture is to use a rectangular surface with inter-antenna spacing far less than half of the wavelength [1] and there exist several candidate hardware implementations [3]. In a planar array, the spatial correlation among the channel fading realizations at different antennas is inevitable and leads to a rank-deficient spatial correlation matrix [6]. In [4], a small-scale fading model for the holographic MIMO channel is analyzed from an electromagnetic perspective. In this letter,

we consider channel modeling by providing an exact integral expression for the spatial correlation matrix with non-isotropic scattering and directive antennas. We derive a closed-form expression suitable for large-scale performance evaluation.

The spatial correlation matrix of a UE should be known at the BS to perform minimum mean-squared error (MMSE) channel estimation. In a holographic massive MIMO system with thousands of antennas, it is complex to both acquire the spatial correlation matrix and implement the MMSE estimator. An alternative is to use the least-square (LS) estimator, which utilizes no channel statistics. However, the performance of LS to MMSE is inferior at low values of the signal-to-noise ratio (SNR). Moreover, the LS scheme neglects the spatial correlation induced by the array geometry, which is naturally known in a given deployment. In this letter, we propose several novel channel estimation schemes that exploit the array geometry to outperform the LS estimator. We motivate our schemes analytically and develop insights based on simulations.

## II. SYSTEM AND CHANNEL MODELING

We consider an uplink holographic massive MIMO system where the BS is equipped with a uniform planar array (UPA) with  $M$  antennas. As illustrated in Fig. 1, the number of antennas per row and per column are denoted by  $M_H$  and  $M_V$ , respectively, and  $M = M_H M_V$ . The horizontal and vertical antenna spacing is  $\Delta$ . We are particularly targeting use cases with thousands of antennas and antenna spacing below half of the wavelength  $\lambda$ . The antennas are indexed row-by-row by  $m \in [1, M]$ , thus the location of the  $m$ th antenna with respect to the origin in Fig. 1 is

$$\mathbf{u}_m = [0, i(m)\Delta, j(m)\Delta]^T \quad (1)$$

where  $i(m) = \text{mod}(m-1, M_H)$  and  $j(m) = \lfloor (m-1)/M_H \rfloor$  are the horizontal and vertical indices of element  $m$ , respectively, on the two-dimensional grid. Notice that  $\text{mod}(\cdot, \cdot)$  denotes the modulus operation and  $\lfloor \cdot \rfloor$  truncates the argument.

Using this notation, if a plane wave is impinging on the UPA from the azimuth angle  $\varphi$  and elevation angle  $\theta$ , the array response vector becomes [2, Sec. 7.3]

$$\mathbf{a}(\varphi, \theta) = [e^{j\mathbf{k}(\varphi, \theta)^T \mathbf{u}_1}, \dots, e^{j\mathbf{k}(\varphi, \theta)^T \mathbf{u}_M}]^T \quad (2)$$

where  $\mathbf{k}(\varphi, \theta) \in \mathbb{R}^3$  is the wave vector

$$\mathbf{k}(\varphi, \theta) = \frac{2\pi}{\lambda} [\cos(\theta) \cos(\varphi), \cos(\theta) \sin(\varphi), \sin(\theta)]^T. \quad (3)$$

We consider an arbitrary single-antenna UE and denote its channel to the BS by  $\mathbf{h} \in \mathbb{C}^M$ . When the UE transmits,

Ö. T. Demir and E. Björnson are with the KTH Royal Institute of Technology, 10044 Stockholm, Sweden ({ozlemt, emilbjo}@kth.se). E. Björnson is also with Linköping University, 58183 Linköping, Sweden.

L. Sanguinetti is with the University of Pisa, Dipartimento di Ingegneria dell'Informazione, 56122 Pisa, Italy (luca.sanguinetti@unipi.it).

This work was supported by the FFL18-0277 grant from the Swedish Foundation for Strategic Research.

the received signal at the BS will generally consist of a superposition of multipath components that can be expanded as a continuum of plane waves [7]. Hence, we can express the channel as

$$\mathbf{h} = \iint_{-\pi/2}^{\pi/2} g(\varphi, \theta) \mathbf{a}(\varphi, \theta) d\theta d\varphi \quad (4)$$

where the *angular spreading function*  $g(\varphi, \theta)$  specifies the gain and phase-shift from each direction  $(\varphi, \theta)$  and  $\mathbf{a}(\varphi, \theta)$  is the array response vector in (2) for  $\varphi \in [-\frac{\pi}{2}, \frac{\pi}{2}]$  and  $\theta \in [-\frac{\pi}{2}, \frac{\pi}{2}]$ . Note that the waves only arrive from directions in front of the array; that is,  $\varphi \in [-\frac{\pi}{2}, \frac{\pi}{2}]$ .

The microscopic fading created by small-scale mobility is captured by  $g(\varphi, \theta)$  being a time-varying variable that can be modeled stochastically. We consider the conventional block fading model, where the channel  $\mathbf{h}$  is constant within one time-frequency block and takes independent realization across blocks from a stationary stochastic distribution. In accordance to [7], we model  $g(\varphi, \theta)$  as a spatially uncorrelated circularly symmetric Gaussian stochastic process with cross-correlation

$$\mathbb{E}\{g(\varphi, \theta)g^*(\varphi', \theta')\} = \beta f(\varphi, \theta)\delta(\varphi - \varphi')\delta(\theta - \theta') \quad (5)$$

where  $\delta(\cdot)$  denotes the Dirac delta function,  $\beta$  denotes the average channel gain (i.e., capturing pathloss and shadowing), and  $f(\varphi, \theta)$  is the normalized *spatial scattering function* [7]. The latter function describes the angular multipath distribution and the directivity gain of the antennas, and it is normalized so that  $\iint f(\varphi, \theta)d\theta d\varphi = 1$ . It thus follows that

$$\mathbf{h} \sim \mathcal{N}_{\mathbb{C}}(\mathbf{0}, \mathbf{R}) \quad (6)$$

which is a correlated Rayleigh fading channel fully characterized by the spatial correlation matrix

$$\mathbf{R} = \mathbb{E}\{\mathbf{h}\mathbf{h}^H\} = \beta \iint_{-\pi/2}^{\pi/2} f(\varphi, \theta) \mathbf{a}(\varphi, \theta) \mathbf{a}^H(\varphi, \theta) d\theta d\varphi \quad (7)$$

where the last equality follows from (5). Notice that  $\text{tr}(\mathbf{R}) = M\beta$ . By utilizing the structure of the array response in (2), we obtain the following general channel model.

**Lemma 1.** *For any given spatial scattering function  $f(\varphi, \theta)$ , the channel vector  $\mathbf{h} \sim \mathcal{N}_{\mathbb{C}}(\mathbf{0}, \mathbf{R})$  of the UPA has the spatial correlation matrix  $\mathbf{R}$  with the  $(m, l)$ th entry given by*

$$[\mathbf{R}]_{m,l} = \beta \iint_{-\pi/2}^{\pi/2} f(\varphi, \theta) \times e^{j2\pi(d_H^{ml} \sin(\varphi) \cos(\theta) + d_V^{ml} \sin(\theta))} d\theta d\varphi \quad (8)$$

where the horizontal and vertical distances between antenna  $m$  and  $l$  (normalized by the wavelength) are given by

$$d_H^{ml} = \frac{(i(m) - i(l)) \Delta}{\lambda}, \quad d_V^{ml} = \frac{(j(m) - j(l)) \Delta}{\lambda}. \quad (9)$$

The double-integral in (8) can be computed numerically for any spatial scattering function, but some functions also lead to closed-form expressions. One example is an *isotropic scattering environment* where the multipath components are

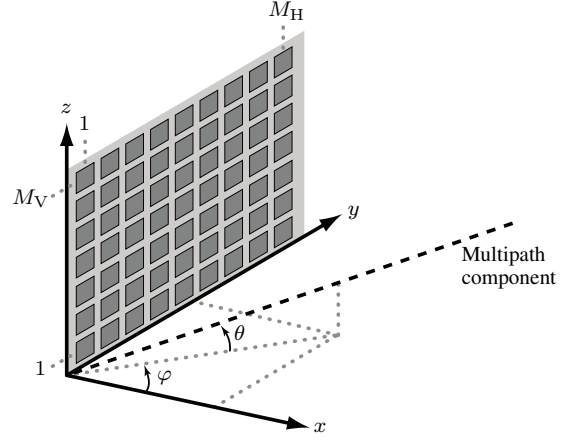


Fig. 1. The 3D geometry of a UPA consisting of  $M_H$  antennas per row and  $M_V$  antennas per column.

equally strong in all directions and the antennas are isotropic (i.e.,  $f(\varphi, \theta) = \cos(\theta)/(2\pi)$ , where the cosine comes from the spherical coordinate system). We denote the resulting correlation matrix by  $\mathbf{R}_{\text{iso}}$  and the  $(m, l)$ th entry is [6]

$$[\mathbf{R}_{\text{iso}}]_{m,l} = \beta \text{sinc} \left( 2\sqrt{(d_H^{ml})^2 + (d_V^{ml})^2} \right) \quad (10)$$

where  $\text{sinc}(x) = \sin(\pi x)/(\pi x)$  is the sinc function. The expression in (10) shows that two antennas that are spaced apart by an integer multiple of  $\lambda/2$  will exhibit mutually uncorrelated fading. However, this can never be satisfied for all pairs of antennas in a UPA [6]. Therefore, such an array will always exhibit spatially correlated fading.

#### A. Clustered Scattering Model with Directive Antennas

We will now develop a spatial correlation matrix model for a realistic scenario with directive antennas and a non-isotropic scattering environment. In particular, the scattered waves from a UE reach the BS from a set of  $N$  angular clusters, which could represent different objects in the environment. This is a generalization of [8, Sec. VIII], where a UPA with a single cluster and isotropic antennas is considered. We consider antennas with a cosine directivity pattern along the azimuth and elevation angles given by [9]

$$\mathcal{D}(\varphi, \theta) \propto \cos^a(\varphi) \cos^b(\theta), \quad \varphi \in \left[-\frac{\pi}{2}, \frac{\pi}{2}\right], \theta \in \left[-\frac{\pi}{2}, \frac{\pi}{2}\right] \quad (11)$$

where the exponents  $a \geq 0$  and  $b \geq 0$  determine the directivity. Larger values result in narrower patterns. The proportionality constant should make  $\iint \mathcal{D}(\varphi, \theta) \cos(\theta) d\varphi d\theta = 4\pi$ .

We assume that cluster  $n$  is centered around the nominal azimuth and elevation angles  $\varphi_n$  and  $\theta_n$ , for  $n = 1, \dots, N$ . Let  $\delta_n$  and  $\epsilon_n$  denote the respective angular deviations. Using an independent von Mises distribution in the considered angle range for the multipath components around the nominal angles [10] and including the directivity pattern from (11), we obtain the spatial scattering function for cluster  $n$  as

$$f(\delta_n, \epsilon_n) = \mathcal{A}_n \cos^a(\varphi_n + \delta_n) \cos^{b+1}(\theta_n + \epsilon_n) \times e^{\frac{\cos(2\delta_n)}{4\sigma_\varphi^2}} e^{\frac{\cos(2\epsilon_n)}{4\sigma_\theta^2}}, \quad |\varphi_n + \delta_n| \leq \frac{\pi}{2}, \quad |\theta_n + \epsilon_n| \leq \frac{\pi}{2} \quad (12)$$

where the scalar  $\mathcal{A}_n > 0$  must be selected so that  $\iint f(\delta_n, \epsilon_n) d\delta_n d\epsilon_n = 1$ . The additional  $\cos(\theta_n + \epsilon_n)$  term comes from the width of a solid angle in the spherical coordinate system. As the angular standard deviations  $\sigma_\varphi$  and  $\sigma_\theta$  go to zero, the von Mises distribution approaches the Gaussian distribution. Using (8) and (12), the  $(m, l)$ th entry of the spatial correlation matrix becomes

$$\begin{aligned} [\mathbf{R}]_{m,l} &= \sum_{n=1}^N \mathcal{A}_n \beta_n \int_{-\theta_n - \pi/2}^{-\theta_n + \pi/2} \int_{-\varphi_n - \pi/2}^{-\varphi_n + \pi/2} e^{j2\pi d_{\text{H}}^{ml} \sin(\theta_n + \epsilon_n)} \\ &\quad \times e^{j2\pi d_{\text{H}}^{ml} \sin(\varphi_n + \delta_n) \cos(\theta_n + \epsilon_n)} \cos^a(\varphi_n + \delta_n) \\ &\quad \times \cos^{b+1}(\theta_n + \epsilon_n) e^{\frac{\cos(2\delta_n)}{4\sigma_\varphi^2}} e^{\frac{\cos(2\epsilon_n)}{4\sigma_\theta^2}} d\delta_n d\epsilon_n \quad (13) \end{aligned}$$

where  $\beta_n \geq 0$  is the average channel gain of cluster  $n$  with  $\sum_{n=1}^N \beta_n = \beta$ . The integrals in (13) can be computed numerically but that is computationally complex for large arrays since  $\mathbf{R}$  has  $M^2$  entries. The following lemma provides a closed-form approximation that is tight for narrow angular clusters. The proof is omitted due to space limitations.

**Lemma 2.** *When the angular deviations are small in the sense that  $\cos(\delta_n) \approx 1$ ,  $\cos(\epsilon_n) \approx 1$ ,  $\sin(\delta_n) \approx \delta_n$ ,  $\sin(\epsilon_n) \approx \epsilon_n$ , for  $n = 1, \dots, N$ , then the  $(m, l)$ th entry of the spatial correlation matrix can be tightly approximated as*

$$\begin{aligned} [\mathbf{R}]_{m,l} &\approx \sum_{n=1}^N \frac{\beta_n}{\cos^a(\varphi_n) \cos^{b+1}(\theta_n)} \frac{A_{mln} \tilde{\sigma}_{mln}}{\sigma_\varphi} e^{-\frac{B_{mln}^2 \tilde{\sigma}_{mln}^2}{2}} \\ &\quad \times e^{\frac{D_{mln}^2 \sigma_\theta^2 (C_{mln}^2 \sigma_\theta^2 \tilde{\sigma}_{mln}^2 - 1)}{2}} e^{-jB_{mln} C_{mln} D_{mln} \sigma_\theta^2 \tilde{\sigma}_{mln}^2} \\ &\quad \times (X_{mln} - Y_{mln} (jB_{mln} \tilde{\sigma}_{mln}^2 - C_{mln} D_{mln} \sigma_\theta^2 \tilde{\sigma}_{mln}^2)) \quad (14) \end{aligned}$$

with  $A_{mln} = e^{j2\pi d_{\text{H}}^{ml} \sin(\varphi_n) \cos(\theta_n)} e^{j2\pi d_{\text{V}}^{ml} \sin(\theta_n)}$ ,  $B_{mln} = 2\pi d_{\text{H}}^{ml} \cos(\varphi_n) \cos(\theta_n)$ ,  $C_{mln} = -2\pi d_{\text{H}}^{ml} \cos(\varphi_n) \sin(\theta_n)$ ,  $D_{mln} = -2\pi d_{\text{H}}^{ml} \sin(\varphi_n) \sin(\theta_n) + 2\pi d_{\text{V}}^{ml} \cos(\theta_n)$ ,  $\tilde{\sigma}_{mln}^2 = \frac{\sigma_\varphi^2}{1 + C_{mln}^2 \sigma_\theta^2 \sigma_\theta^2}$ ,  $X_{mln} = \cos^a(\varphi_n) (\cos^{b+1}(\theta_n) - j(b+1) \cos^b(\theta_n) \sin(\theta_n) \sigma_\theta^2 D_{mln})$ ,  $Y_{mln} = a \cos^{a-1}(\varphi_n) \sin(\varphi_n) \cos^{b+1}(\theta_n) + j\sigma_\theta^2 (b+1) \cos^b(\theta_n) \times \sin(\theta_n) (\cos^a(\varphi_n) C_{mln} - a \cos^{a-1}(\varphi_n) \sin(\varphi_n) D_{mln})$ .

In Fig. 2, the tightness of the approximate closed-form expression in Lemma 2 is demonstrated. The eigenvalues of the exact and approximate spatial correlation matrices are plotted in decreasing order. We consider a  $64 \times 64$  UPA with the antennas having a cosine pattern proportional to  $\cos(\varphi) \cos(\theta)$ . There are  $N = 6$  clusters with equal power gains. The nominal azimuth angles are uniformly selected between  $-40^\circ$  and  $60^\circ$  in  $20^\circ$  steps. The nominal elevation angles are uniformly selected between  $-35^\circ$  and  $-10^\circ$  in  $5^\circ$  steps. The angular standard deviations are  $\sigma_\varphi = \sigma_\theta = 5^\circ$ . The filled circles in Fig. 2 shows the effective rank, containing a fraction  $1 - 10^{-5}$  of the sum of all eigenvalues. Fig. 2 shows that the eigenvalues match closely with differences only in the lower tails of the curves, corresponding to eigenvalues that are five orders-of-magnitude below the maximum ones. The gap reduces with smaller antenna spacing  $\Delta$ . This demonstrates the tightness of the approximated closed-form in Lemma 2.

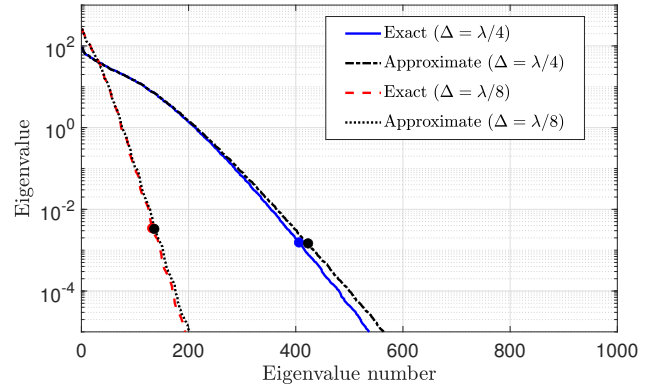


Fig. 2. Sorted eigenvalues for the exact and approximate spatial correlation matrices. A  $64 \times 64$  UPA with varying antenna spacings is considered.

### III. CHANNEL ESTIMATION

The BS must estimate the channel realization  $\mathbf{h}$  in each coherence block to use its  $M$  antennas for coherent beamforming. The standard approach is that the UE sends a predefined pilot sequence. The received signal at the BS is modeled as [2, Sec. 3]

$$\mathbf{y} = \sqrt{\rho} \mathbf{h} + \mathbf{n} \quad (15)$$

where  $\rho > 0$  is the pilot SNR and the receiver noise is distributed as  $\mathbf{n} \sim \mathcal{N}_{\mathbb{C}}(\mathbf{0}, \mathbf{I}_M)$ .

Different channel estimation methods can be utilized at the BS, depending on the available statistical information. If the full spatial correlation matrix  $\mathbf{R}$  in (7) is known, then the MMSE estimate of  $\mathbf{h}$  is

$$\hat{\mathbf{h}}_{\text{MMSE}} = \sqrt{\rho} \mathbf{R} (\rho \mathbf{R} + \mathbf{I}_M)^{-1} \mathbf{y}. \quad (16)$$

However, since  $\mathbf{R}$  contains  $M^2$  entries, it is challenging to acquire it in practice, particularly when  $M$  is large and/or when the UE is only transmitting a small data packet.

An alternative approach is to utilize the LS estimator that only requires knowledge of the pilot SNR,  $\rho$ . The LS estimate of  $\mathbf{h}$  is given by

$$\hat{\mathbf{h}}_{\text{LS}} = \frac{\mathbf{y}}{\sqrt{\rho}}. \quad (17)$$

We will show that this estimator is unnecessarily conservative.

#### A. Subspace-Based Channel Estimation

The rank of the spatial correlation matrix  $\mathbf{R}_{\text{iso}}$  for isotropic scattering and antennas is approximately  $\pi M (\Delta/\lambda)^2$  when  $M$  is large and  $\Delta$  is small [6, Prop. 2]. For example, for  $\Delta = \lambda/2$ , the rank is  $M\pi/4$ , thus 21% of the eigenvalues are zero. The rank-deficiency grows when the antenna spacing reduces due to the resulting spatial oversampling; 80% of the eigenvalues are zero when using  $\Delta = \lambda/4$ . With non-isotropic scattering and/or non-isotropic antennas, we might obtain even stronger rank-deficiency. However, since the low rank of  $\mathbf{R}_{\text{iso}}$  is caused purely by spatial oversampling, an interesting question is: Can we utilize the array geometry to improve the channel estimation when the true correlation matrix  $\mathbf{R}$  is unknown?

In this subsection, we will develop a subspace-based estimation method that outperforms LS estimation without requiring

any UE-dependent prior information but only the array geometry. We will first show how the MMSE estimator implicitly exploits low-rank correlation matrices. We let  $1 \leq r \leq M$  denote the rank of  $\mathbf{R}$ , i.e.,  $\text{rank}(\mathbf{R}) = r$ . The compact eigenvalue decomposition is denoted as  $\mathbf{R} = \mathbf{U}_1 \mathbf{\Lambda}_1 \mathbf{U}_1^H$ , where the diagonal matrix  $\mathbf{\Lambda}_1 \in \mathbb{C}^{r \times r}$  contains the non-zero eigenvalues and the columns of  $\mathbf{U}_1 \in \mathbb{C}^{M \times r}$  contains the corresponding orthonormal eigenvectors. The channel  $\mathbf{h}$  can be expressed as  $\mathbf{h} = \mathbf{R}^{\frac{1}{2}} \mathbf{v} = \mathbf{U}_1 \mathbf{\Lambda}_1^{\frac{1}{2}} \mathbf{v}$ , where  $\mathbf{v} \sim \mathcal{N}_{\mathbb{C}}(\mathbf{0}, \mathbf{I}_r)$ . Hence, all channel realizations exist in the subspace spanned by  $\mathbf{U}_1$  (i.e., they are linear combinations of its columns).

The MMSE estimate  $\hat{\mathbf{h}}_{\text{MMSE}}$  in (16) can be expressed as

$$\hat{\mathbf{h}}_{\text{MMSE}} = \mathbf{U}_1 \left( \frac{1}{\sqrt{\rho}} \mathbf{D}_1 \right) \mathbf{U}_1^H \mathbf{y} \quad (18)$$

where  $\mathbf{D}_1 = \rho \mathbf{\Lambda}_1 (\rho \mathbf{\Lambda}_1 + \mathbf{I}_r)^{-1}$  is a diagonal matrix. Hence, the MMSE estimator in (18) carries out three operations: 1)  $\mathbf{U}_1^H \mathbf{y}$  projects the received signal onto the subspace spanned by  $\mathbf{U}_1$ ; 2) The resulting  $r$  channel dimensions are MMSE estimated using the scaling factors in  $\mathbf{D}_1 / \sqrt{\rho}$ ; 3) The estimate is brought back to the original  $M$ -dimensional space using  $\mathbf{U}_1$ .

If only the subspace spanned by  $\mathbf{U}_1$  is known, not the eigenvalues necessary to compute  $\mathbf{D}_1$ , we can replace  $\mathbf{D}_1$  in (18) by the corresponding LS estimator. We call this the *reduced-subspace LS (RS-LS)* estimator:

$$\hat{\mathbf{h}}_{\text{RS-LS}} = \frac{\mathbf{U}_1 \mathbf{U}_1^H \mathbf{y}}{\sqrt{\rho}}. \quad (19)$$

We notice that RS-LS is obtained from the MMSE estimator by replacing  $\mathbf{D}_1$  with  $\mathbf{I}_r$ . Moreover, we notice that  $\mathbf{D}_1 \rightarrow \mathbf{I}_r$  as  $\rho \rightarrow \infty$ , thus we expect RS-LS to perform similarly as MMSE at high SNR, but to provide larger estimation errors in other situations. In any case, the subspace projection in RS-LS removes the noise from  $M - r$  dimensions, effectively increasing the SNR by a factor  $M/r$  in the estimation phase.

To dispense from knowledge of  $\mathbf{R}$ , we can instead utilize RS-LS along with some other correlation matrix  $\bar{\mathbf{R}}$  that is not representing a particular UE but the general array geometry. For example, we can set  $\bar{\mathbf{R}} = \mathbf{R}_{\text{iso}}$  to ensure that all  $\text{rank}(\mathbf{R}_{\text{iso}})$  possible channel dimensions are considered by the estimator. This property can be formalized as follows.

**Lemma 3.** *Let  $\bar{\mathbf{R}}$  and  $\mathbf{R}$  be two spatial correlation matrices obtained using the same array geometry. The spatial scattering functions corresponding to these correlation matrices are denoted by  $\bar{f}(\varphi, \theta)$  and  $f(\varphi, \theta)$ , respectively, for  $\varphi \in [-\pi/2, \pi/2]$  and  $\theta \in [-\pi/2, \pi/2]$ . Assume that  $\bar{f}(\varphi, \theta)$  and  $f(\varphi, \theta)$  are either continuous at each point on its domain or contain Dirac delta functions.*

*If the domain of  $\bar{f}(\varphi, \theta)$  for which  $\bar{f}(\varphi, \theta) > 0$  contains the domain  $f(\varphi, \theta)$  for which  $f(\varphi, \theta) > 0$ , then the subspace spanned by the columns of  $\bar{\mathbf{R}}$  contains the subspace spanned by the columns of  $\mathbf{R}$ .*

*Proof.* The proof is given in the appendix.  $\square$

An important special case of Lemma 3 is obtained for  $\bar{\mathbf{R}} = \mathbf{R}_{\text{iso}}$  by noting that the span of the correlation matrix with

isotropic scattering spans the entire angular domain. Hence, for a given array geometry, the subspace spanned by the columns of  $\mathbf{R}_{\text{iso}}$  contains the subspace spanned by any other spatial correlation matrix  $\mathbf{R}$ .

For a given  $\bar{\mathbf{R}}$  that satisfies the condition in Lemma 3, the resulting so-called *conservative RS-LS* estimator is

$$\hat{\mathbf{h}}_{\text{RS-LS}}^{\text{conserv}} = \frac{\bar{\mathbf{U}}_1 \bar{\mathbf{U}}_1^H \mathbf{y}}{\sqrt{\rho}} \quad (20)$$

where the columns  $\bar{\mathbf{U}}_1 \in \mathbb{C}^{M \times \bar{r}}$  are the orthonormal eigenvectors corresponding to the  $\bar{r}$  non-zero eigenvalues of  $\bar{\mathbf{R}}$ .

### B. Discrete Fourier Transform Approximation of the Spatial Correlation Subspace

For the conservative RS-LS method, another simpler alternative is to use a portion of the two-dimensional discrete Fourier transform (DFT) matrix as  $\bar{\mathbf{U}}_1$ . Based on the Fourier plane-wave series expansion in [4, Sec. V.A], the channel from UE to the BS antenna  $m$  can be approximated as

$$[\mathbf{h}]_m \approx \sum_{(\ell_H, \ell_V) \in \mathcal{E}} \alpha_{\ell_H \ell_V} e^{j2\pi \left( \frac{i(m)\ell_H}{M_H} + \frac{j(m)\ell_V}{M_V} \right)} \quad (21)$$

with

$$\mathcal{E} = \left\{ (\ell_H, \ell_V) \in \mathbb{Z}^2 : \left( \frac{\ell_H \lambda}{M_H \Delta} \right)^2 + \left( \frac{\ell_V \lambda}{M_V \Delta} \right)^2 \leq 1 \right\} \quad (22)$$

for a compact spatially-continuous planar surface and  $\min(M_H, M_V) \Delta / \lambda \rightarrow \infty$ . The random variables  $\alpha_{\ell_H \ell_V}$  are independent and zero-mean complex Gaussian distributed. From (21), we can approximate  $\bar{\mathbf{U}}_1$  in (20) as the portion of the two-dimensional  $M \times M$  DFT matrix with  $|\mathcal{E}|$  columns whose  $m$ th entry is given by  $e^{j2\pi \left( \frac{i(m)\ell_H}{M_H} + \frac{j(m)\ell_V}{M_V} \right)} / \sqrt{M}$  for  $(\ell_H, \ell_V) \in \mathcal{E}$ . The advantage of using the DFT approximation in the conservative RS-LS method is that there is no need to compute the eigenvalue decomposition of  $\bar{\mathbf{R}}$ . The DFT approximation-based RS-LS method is computationally much cheaper and it captures all the degrees of freedom asymptotically.

## IV. COMPARISON OF CHANNEL ESTIMATION SCHEMES

We will now quantify the channel estimation performance of the considered schemes numerically in terms of the normalized mean-square error (NMSE). We use mainly the same setup as in Fig. 2 with  $128 \times 128$  UPA and plot the NMSE versus SNR,  $\rho$ , with  $\beta = 1$ . The MMSE, LS, RS-LS, and Isotropic-RS-LS are obtained from (16), (17), (19), and (20) with  $\mathbf{R}_{\text{iso}}$ , respectively. The DFT-RS-LS uses the DFT approximation from Section III-B in the conservative RS-LS method in (20).

The antenna spacing is  $\Delta = \lambda/4$  in Fig. 3. The optimal MMSE estimator provides the lowest NMSE, while the conventional statistics-unaware LS estimator provides a 10 dB higher NMSE. The proposed RS-LS estimator applies LS within the subspace spanned by the true spatial correlation matrix, thereby eliminating noise from the nullspace of the correlation matrix. As the SNR increases, the gap between

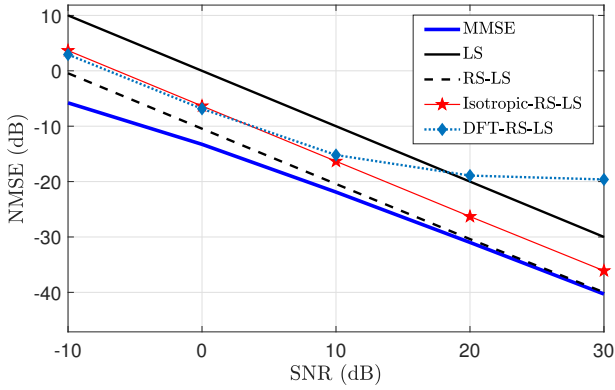


Fig. 3. NMSE versus SNR for the  $128 \times 128$  UPA with  $\Delta = \lambda/4$ .

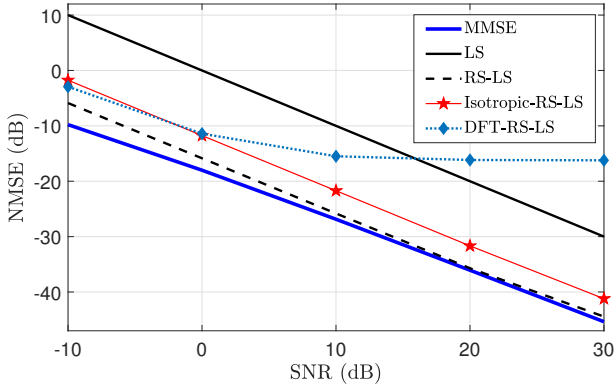


Fig. 4. NMSE versus SNR for the  $128 \times 128$  UPA with  $\Delta = \lambda/8$ .

RS-LS and MMSE vanishes. However, RS-LS still uses the true correlation matrix. The proposed estimators “Isotropic-RS-LS” and “DFT-RS-LS” are not utilizing such information but only the array geometry. Isotropic-RS-LS provides a 6 dB performance gain over LS, but there is a gap to RS-LS. The reason is that the true correlation matrix has lower rank than  $\mathbf{R}_{\text{iso}}$  (the effective ranks are 1481 versus 3808).

DFT-RS-LS provides almost the same NMSE as Isotropic-RS-LS for SNRs below 10 dB, but then features a saturation effect. This is because the DFT approximation is not capturing the complete eigenspace of this finite-dimensional channel, even if it asymptotically matches the subspace of any spatial correlation matrix. However, DFT-RS-LS provides a rather high-quality channel estimator (NMSE close to  $-20$  dB) without the need for an eigendecomposition, unlike Isotropic-RS-LS.

We reduce the antenna spacing to  $\Delta = \lambda/8$  in Fig. 4. Since the array is denser, the ratio of the rank of the spatial correlation matrix to  $M$  is smaller and the NMSE gap between Isotropic-RS-LS and LS increases to 11 dB. Since the array area is now smaller than in Fig. 3, the accuracy of the DFT approximation reduces and the gap between DFT-RS-LS and Isotropic-RS-LS increases.

## V. CONCLUSIONS

We have derived a closed-form spatial correlation matrix expression for planar holographic massive MIMO arrays with clustered scattering and directive antennas. Since the antennas

are densely deployed, the spatial correlation matrices become strongly rank-deficient, even when having isotropic scattering. We have proposed several channel estimation schemes that exploit the rank-deficiency induced by the array geometry without requiring the exact channel statistics. These estimators outperform the conventional statistics-unaware LS estimator. The SNR gain is 10 dB when 10% of the eigenvalues are non-zero. At low SNR, the low-rank subspaces can be identified from a DFT approximation, leading to even lower complexity.

## APPENDIX: PROOF OF LEMMA 3

We consider an arbitrary vector  $\mathbf{x} \in \mathbb{C}^M$  that is in the null space of  $\bar{\mathbf{R}}$ . If we can show that  $\mathbf{x}$  is also in the null space of  $\mathbf{R}$ , we have completed the proof. We have

$$\mathbf{x}^H \bar{\mathbf{R}} \mathbf{x} = \beta \iint_{\bar{\mathcal{F}}} \bar{f}(\varphi, \theta) |\mathbf{x}^H \mathbf{a}(\varphi, \theta)|^2 d\theta d\varphi = 0 \quad (23)$$

where we have used (7) and  $\bar{\mathcal{F}}$  is the domain of  $\bar{f}(\varphi, \theta)$  where it is non-zero. If  $\bar{f}(\varphi, \theta)$  includes some Dirac delta impulses, then we should have  $\mathbf{x}^H \mathbf{a}(\varphi, \theta) = 0$  at the corresponding angles  $(\varphi, \theta) \in \bar{\mathcal{F}}$  to satisfy (23). At the other angles where  $\bar{f}(\varphi, \theta)$  is continuous, we first assume there is at least one pair of angles  $(\varphi^*, \theta^*) \in \bar{\mathcal{F}}$  with  $\mathbf{x}^H \mathbf{a}(\varphi^*, \theta^*) \neq 0$ . Then we can find a region of  $\bar{\mathcal{F}}$  around  $(\varphi^*, \theta^*)$  such that  $\mathbf{x}^H \mathbf{a}(\varphi, \theta) \neq 0$  from the continuity. This assumption results in a positive integral in (23), which violates the initial assumption that the integral is zero. Hence,  $\mathbf{x}$  should be orthogonal to  $\mathbf{a}(\varphi, \theta)$ ,  $\forall (\varphi, \theta) \in \bar{\mathcal{F}}$ , and hence  $\forall (\varphi, \theta) \in \mathcal{F}$  where  $\mathcal{F}$  is the domain of  $f(\varphi, \theta)$  for which it is non-zero. This in turn leads to the fact that  $\mathbf{x}^H \mathbf{R} \mathbf{x} = 0$  from (7) and completes the proof.

## REFERENCES

- [1] E. Björnson, L. Sanguinetti, H. Wymeersch, J. Hoydis, and T. L. Marzetta, “Massive MIMO is a reality—What is next? Five promising research directions for antenna arrays,” *Digital Signal Processing*, vol. 94, pp. 3–20, Nov. 2019.
- [2] E. Björnson, J. Hoydis, and L. Sanguinetti, “Massive MIMO networks: Spectral, energy, and hardware efficiency,” *Foundations and Trends® in Signal Processing*, vol. 11, no. 3-4, pp. 154–655, 2017.
- [3] C. Huang, S. Hu, G. C. Alexandropoulos, A. Zappone, C. Yuen, R. Zhang, M. Di Renzo, and M. Debbah, “Holographic MIMO surfaces for 6G wireless networks: Opportunities, challenges, and trends,” *IEEE Wireless Communications*, vol. 27, no. 5, pp. 118–125, 2020.
- [4] A. Pizzo, T. L. Marzetta, and L. Sanguinetti, “Spatially-stationary model for holographic MIMO small-scale fading,” *IEEE Journal on Selected Areas in Communications*, vol. 38, no. 9, pp. 1964–1979, 2020.
- [5] S. Hu, F. Rusek, and O. Edfors, “Beyond massive MIMO: The potential of data transmission with large intelligent surfaces,” *IEEE Transactions on Signal Processing*, vol. 66, no. 10, pp. 2746–2758, 2018.
- [6] E. Björnson and L. Sanguinetti, “Rayleigh fading modeling and channel hardening for reconfigurable intelligent surfaces,” *IEEE Wireless Communications Letters*, vol. 10, no. 4, pp. 830–834, 2021.
- [7] A. Sayeed, “Deconstructing multiantenna fading channels,” *IEEE Trans. Signal Process.*, vol. 50, no. 10, pp. 2563–2579, 2002.
- [8] Ö. T. Demir and E. Björnson, “Is channel estimation necessary to select phase-shifts for RIS-assisted massive MIMO?” *CoRR*, vol. abs/2106.09770, 2021.
- [9] A. Kumar, J. Bartelt, A. N. Barreto, and G. Fettweis, “2D active antenna array design for mMIMO to improve spectral and energy efficiency,” in *IEEE 2nd 5G World Forum (5GWF)*, 2019, pp. 490–495.
- [10] A. Abdi and M. Kaveh, “A space-time correlation model for multielement antenna systems in mobile fading channels,” *IEEE Journal on Selected Areas in communications*, vol. 20, no. 3, pp. 550–560, 2002.